Ultrasound in Medicine & Biology 49 (2023) 1415–1421

Contents lists available at ScienceDirect

Ultrasound in Medicine & Biology

journal homepage:

Original Contribution

High-Speed Imaging of Microsphere Transport by Cavitation Activity in a Tissue-Mimicking Phantom

Jonathan Vince [a], Andrew Lewis [b], Eleanor Stride [a,*]

[a] Institute of Biomedical Engineering, Department of Engineering Science, University of Oxford, Oxford, UK
[b] Alchemed Bioscience Consulting Ltd., Stable Cottage, Farnham, Surrey, UK

ARTICLE INFO

Keywords:
Cavitation
High-speed imaging
Therapeutic ultrasound
Embolic microspheres
Extravasation

Objective: Ultrasound-mediated cavitation has been harnessed to improve the delivery of various therapeutics, including the extravasation of small molecule drugs and nanoparticles (<1 μm) into soft tissue. This study investigated whether cavitation could also enhance the extravasation of larger (>10 μm) therapeutic particles, representative of radio- or chemo-embolic particles, in a tissue-mimicking phantom.
Methods: High-speed (10^3–10^6 frames/s) optical imaging was used to observe the motion of glass microspheres with diameters of 15–32 or 105–107 μm in an agar phantom under exposure to high-intensity focused ultrasound (0.5 MHz) at a range of peak negative pressures (1.9–2.8 MPa) in the presence of SonoVue microbubbles.
Results: In contrast to the microstreaming reported to be responsible for nanoparticle transport, the formation and translation of bubble clouds were found to be primarily responsible for the motion of glass microspheres. The bubble clouds were seen both to create channels in the phantom and to travel along them under the action of primary acoustic radiation force, either propelling or entraining microspheres with them. Collisions between microspheres were also seen to promote cloud formation and cavitation activity.
Conclusion: Ultrasound-mediated cavitation can promote the transport of solid microparticles in tissue-mimicking material. Further work is needed to understand the influence of tissue mechanical properties and ultrasound exposure parameters on the extent and uniformity of particle distribution that can be achieved.

Introduction

Ultrasound-mediated cavitation has been reported to enhance the transport of various therapeutics [1]—small molecule drugs [2,3], proteins [4,5], viruses [6] and nanoparticles [7–11]—both *in vitro* and in small animal models [12–15]. It has also been used clinically to successfully enhance delivery of chemotherapy across the blood–brain barrier [16–19] for the treatment of pancreatic cancer [20–22] and to augment radiotherapy through tissue sensitisation [23]. To the best of the authors' knowledge, however, there has been no investigation of cavitation facilitating transport of larger particles (0.01–1 mm), such as embolic microspheres used in transarterial chemo-embolization or selective internal radiation therapy.

Clinically, these microspheres are delivered to the tumour vasculature via an intra-arterial catheter or could potentially be injected following surgical removal of a tumour to deliver localised therapy. There are no methods currently, however, that enable physicians to control the spatial distribution of radioactive microspheres post-delivery or to achieve microsphere extravasation. This limits treatment efficacy and increases the risk of off-target delivery, as there is no way of ensuring that a uniform dose of chemotherapy or radiation is delivered throughout the tumour. The overall aim of this study was therefore to investigate whether ultrasound-mediated cavitation could be used to promote the transport of microspheres and hence potentially address this challenge. The secondary objective was to identify the mechanism (s) responsible and compare these with the phenomena observed in cavitation-mediated nanoparticle transport. Please note that these mechanisms are reviewed in the Results and Discussion section together with the relevant background literature.

Methods

Tissue-mimicking phantom

As the aim of this study was to explore the feasibility of microsphere transport by cavitation, a very simple tissue-mimicking phantom was used to ensure optical clarity and consistency of material properties between experiments. The phantom consisted of a rectangular block of agar cast in an acrylic mould (80 × 40 × 40 mm) with removable sides. A stainless-steel rod (4 mm in diameter with a 10-mm section at one end with a 1-mm diameter) was used to create a stepped cylindrical cavity to provide a very basic representation of a section of blood vessel or a cavity formed by surgical resection.

* Corresponding author. Institute of Biomedical Engineering, University of Oxford, Old Road Campus Research Building, Oxford OX3 7DQ, UK
E-mail address: eleanor.stride@eng.ox.ac.uk (E. Stride).

https://doi.org/10.1016/j.ultrasmedbio.2023.01.025
Received 28 July 2022; Revised 20 December 2022; Accepted 30 January 2023

As one of the potential applications of interest is treatment of brain tumours, an agar–agar hydrogel was selected as having physical properties similar to those of glioblastoma multiforme tumour masses [24]. A suspension of agar (0.5% w/v, 500–1500 Da; No. w201201, Sigma Aldrich, St. Louis, MO, USA) in de-ionised water (Millipore-Q Type 1) was de-gassed under reduced pressure for 90 min. It was then microwave irradiated for 390 s to dissolve the agar (>85°C), poured into the mould and set at 4°C for a minimum of 12 h before use. Once set, the front, rear and top faces of the acrylic mould were replaced with acoustically transparent Mylar sheets to allow ultrasound propagation into the phantom.

Microspheres and microbubbles

Glass microspheres with diameters of either 15–32 or 105–107 μm were provided by MoSci (Rolla, MO, USA). These were produced in that the same way as the commercial radio-embolic agent TheraSphere, giving them identical surface properties and density, but they were not irradiated and were made with black glass to provided increased brightfield contrast for the high-speed imaging experiments. Sonovue® (Bracco Research, Zurich, Switzerland) microbubbles were used undiluted to mimic injection into a post-resection cavity.

Water tank and ultrasound exposure

The phantom was immersed in a transparent acrylic water tank (445 × 445 × 175 mm) filled with de-gassed, de-ionised water and connected via an aluminium rod to a manual xyz movement stage (Newport, MKS Instruments, Andover, MS, USA) mounted above the tank, enabling the phantom to be positioned as required. A high-intensity focused ultrasound (HIFU) transducer (H107, Sonic Concepts Bothell, WA, USA) was also suspended in the tank on a fixed assembly. The HIFU transducer had an outer diameter of 64 mm, a centre frequency of 0.5 MHz and a central rectangular cut out measuring 48 × 17 mm.

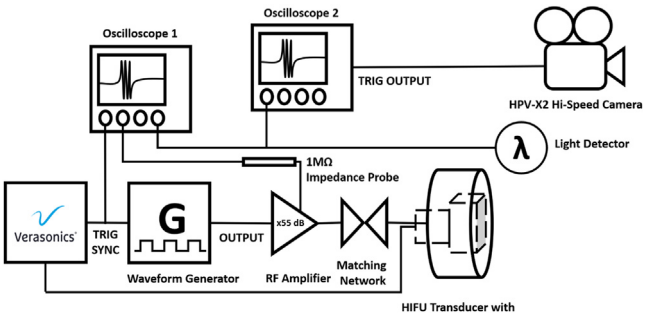

Figure 1. Experimental setup for high-speed optical imaging of microsphere transport in a tissue-mimicking phantom. RF, radiofrequency.

The stainless steel rod used to create the phantom cavity was initially left in place to enable alignment of the transducer foci with the centre of the cavity. A pulser–receiver (JSR Ultrasonics DPR300, Imaginant, Pittsford, NY, USA) connected to the HIFU transducer and an oscilloscope (Le Croy HDO4024, Teledyne, Thousand Oaks, CA, USA) were used to transmit a short, low-amplitude pulse, and the transducer position was adjusted in sub-millimetre increments until the amplitude of the received signal was maximised. The phantom was then removed from

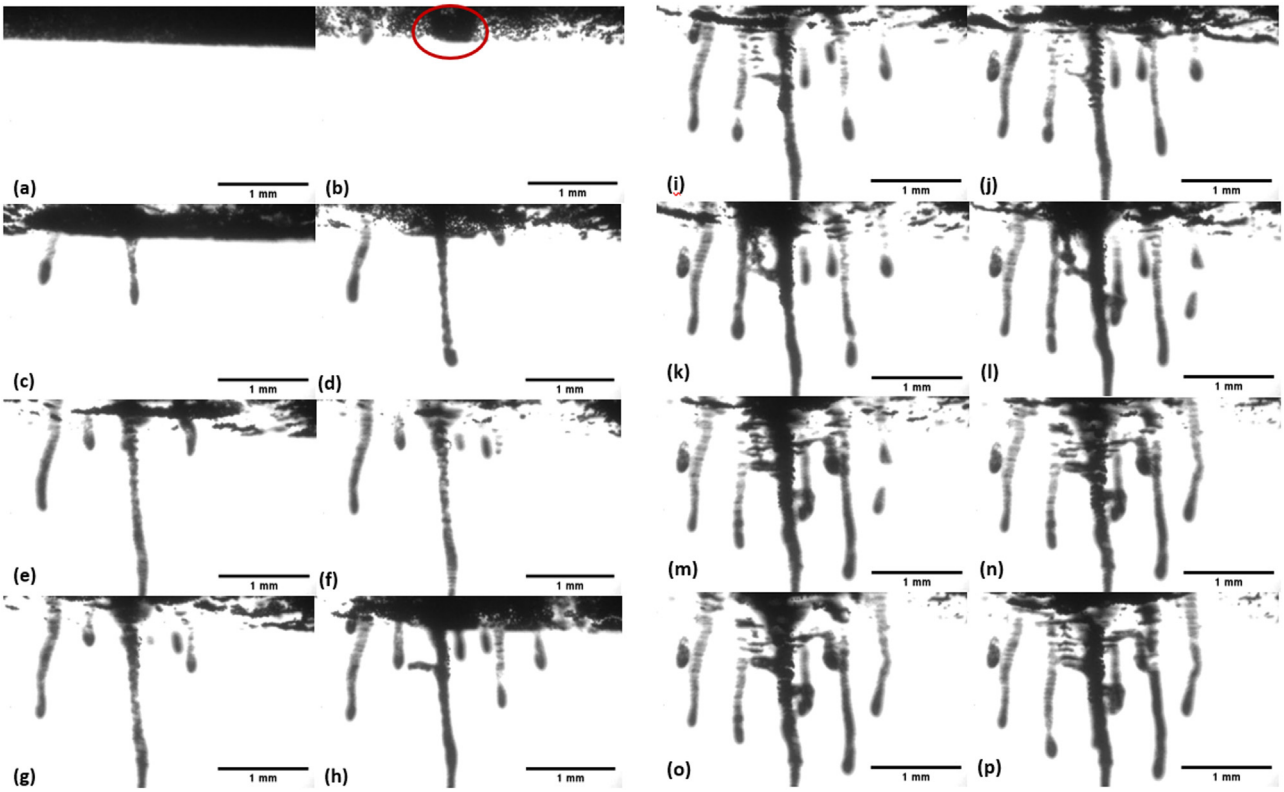

Figure 2. Series of frames (a–p) from high-speed video recordings (Video S1) of the extravasation of black glass microspheres (15–32 μm in diameter) captured with a 4 × objective during ultrasound exposure (0.5 MHz pulse centre frequency, 1.9 MPa peak negative focal pressure, 5% duty cycle, 3.3 Hz pulse repetition frequency). Each image is the last frame of 256-frame video sequences taken at 2000 frames/s approximately 5 s apart over ~80 s. Twenty micrograms of microspheres was injected into the phantom cavity with 310 μL of reconstituted SonoVue microbubbles (~3×10^8 bubbles). The upper edge of the image corresponds to the edge of the cavity closest to the transducer; that is, the direction of ultrasound propagation is from top to bottom. Gravity acts perpendicular to the plane of the image, preventing microspheres from sinking into the channels. Please note that at 4 × magnification, the SonoVue microbubbles are not visible.

the tank, the stainless steel rod was withdrawn and a mixed suspension of microspheres (with diameter/ranges of 15–32 or 106–107 μm) with or without 270 μL of SonoVue was injected into the phantom cavity. The top of the cavity was sealed with a rubber bung, and the phantom replaced in the water tank.

For the microsphere transport experiments, the HIFU transducer was driven at 0.5 MHz using a Verasonics Vantage 256 channel ultrasound research system (Verasonics Inc., Redmond, WA, USA) as an arbitrary waveform generator and a power amplifier (55 dB gain, 1140LA, E&I, Rochester, NY, USA) . The phantom cavity was exposed to a peak negative pressure of either 1.9 or 2.8 MPa, with a 5% duty cycle (DC) and 3.3 Hz pulse repetition frequency (PRF). These exposure conditions were based upon pilot experiments performed to identify the peak negative pressures (PNPs) required for microsphere transport. Transducer calibrations were performed using either a needle or fibre-optic hydrophone (see Figure S1-S3 supplementary material, online only). All of the experiments were performed at a room temperature of ~20°C. A schematic of the experimental setup is provided in Figure 1.

High-speed imaging

To capture cavitation events at a sufficient rate, a Hypervision HPV-X2 (Shimadzu, Tokyo, Japan) high-speed camera was used. The HPV-X2 is capable of recording from 60 to 10 million frames/s, with variable exposure times, and can record a maximum of 256 frames within a single capture. A Solis High-Power LED (445 nm Royal Blue, 48.3 mm clear aperture, 5.4 W, Thor Labs, Cambridge, UK) with a Plug-and-Play Solis LED driver was placed beneath the tank to provide the necessary illumination. A 25 mm ID lens tube (Thor Labs), with a 552 nm edge LaserMUX single-edge laser dichroic beam splitter lens (LM01-552-25, Semrock, Rochester, NY, USA) was attached to the front of the camera connected to a 30 mm Cage-Compatible, Kinematic Fluorescence Filter

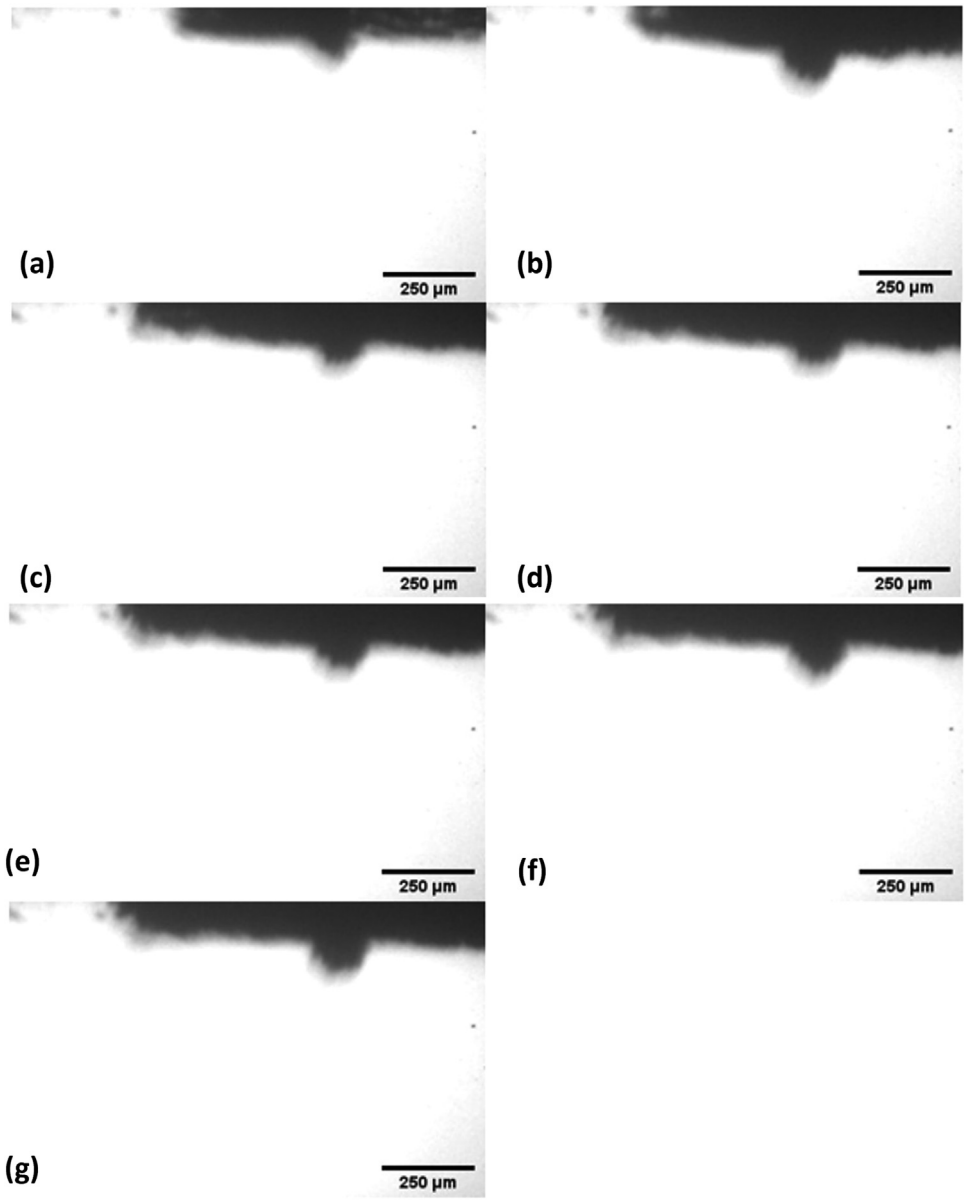

Figure 3. Higher magnification (10 ×) images of the rippling of the phantom cavity wall indicating the presence of a microbubble cloud. (a–g) Frames 132, 201, 240, 244, 248, 252 and 256 of a single video capture (Video S2). The time between frames was 250 ns (total recording time: 2560 μs). The packing of the <15 μm diameter microspheres within the cavity prevented more detailed observation of bubble activity in this case. The direction of ultrasound propagation is from the top to the bottom of each image.

Cube (DFM1T1, Thor Labs) allowing for a 90° reflection to be transmitted to the camera.

An adaptor ring was fitted to the base of the filter cube for attachment of one of two NIKON (Tokyo, Japan) CFI Plan Fluor series air objectives: a 4 × (0.13 NA, 17.2 mm WD) or a 10 × (0.30 NA, 16.00 mm WD). Unfortunately, a water immersible objective of the correct magnification and working distance could not be sourced. and the objectives were therefore inserted into a 100 mL borosilicate glass beaker, which was immersed in the tank to enable imaging without damage to the objectives.

Pilot experiments indicated that microsphere motion occurred after a variable multi-second delay after the start of the ultrasound exposure. This posed a challenge for triggering the high-speed camera. The size and optical contrast of the microspheres enabled them to be observed by the naked human eye, but manually triggering the high-speed camera was not feasible for imaging frame rates above 10,000 fps. A light detector (PDA36A2 Si Switchable gain detector, 400–1000 nm, Thor Labs) was therefore used to detect microsphere movement by monitoring changes in light transmission through the phantom. The signal by the detector was sent to two oscilloscopes (Le Croy HDO4024 and WaveSurfer 2014z, both supplied by Teledyne). The first oscilloscope enabled monitoring of the signal amplitude and phase. The second was used to trigger the recording on the high-speed camera when the signal dropped below an empirically determined threshold.

Results and discussion

Observations of microsphere extravasation

Microsphere extravasation was observed when the peak negative pressure exceeded 1.9 MPa for the smaller microspheres (15–32 μm) and 2.8 MPa for the larger microspheres (106–107 μm). Please note that the term *extravasation* here is used to describe movement of the microspheres out of the cavity into the surrounding phantom matrix. At lower pressures and/or in the absence of SonoVue, there was negligible microsphere transport outside the phantom cavity.

Figure 2 illustrates an example of microsphere (15–32 μm) transport produced by ultrasound-induced cavitation observed under low magnification (4 ×). The series of images illustrates the evolution of the channels in the phantom matrix. Figure 2b depicts an initial disruption to the packing of the microspheres, presumably brought about by the ultrasound-induced motion of a microbubble cloud, that is, a collection of microbubbles forming a cluster that moves as a single entity despite the microbubbles themselves remaining discrete. With each new pulse, a group of microspheres were seen to collide with the cavity boundary and initiate a channel (Fig. 2c; Video S1, online only). As the ultrasound exposure continued and further microsphere collisions occurred, these channels extended in the direction of the applied ultrasound field and more channels formed (Fig. 2d–p). A single tightly packed bolus of microspheres can be seen at the tip of each channel, with a varying number of microspheres distributed along the rest of its length. With each successive pulse, the channels increasingly filled with further microspheres.

The majority of the channels were formed on the side of the cavity opposite the transducer and aligned approximately directly with ultrasound propagation. In some cases, though, the phantom matrix was also disrupted in the pre-focal region. Qualitatively similar results were obtained with both sizes of microsphere. In the example in Figure 2, microsphere transport continued beyond the edge of the image frame (the height of the frame is 2.2 mm) in the direction of ultrasound propagation for several millimeters. The longer the ultrasound was applied, the greater was the length of the channels. As might be expected, those channels most closely aligned with the central axis of ultrasound propagation grew the fastest, regardless of the order in which the channels were initially formed and became most densely packed with microspheres. Interestingly, in channels with a lower density of microspheres, a loose banding was observed. This is discussed further in the supplementary material (online only).

Mechanisms of microsphere extravasation

The videos obtained in this study indicate that microsphere extravasation occurred primarily as the result of microbubble cloud activity rather than the action of individual microbubbles. This is in contrast to the mechanisms reported to be responsible for transport of smaller therapeutics [25,26] and to movement of particles induced by the formation

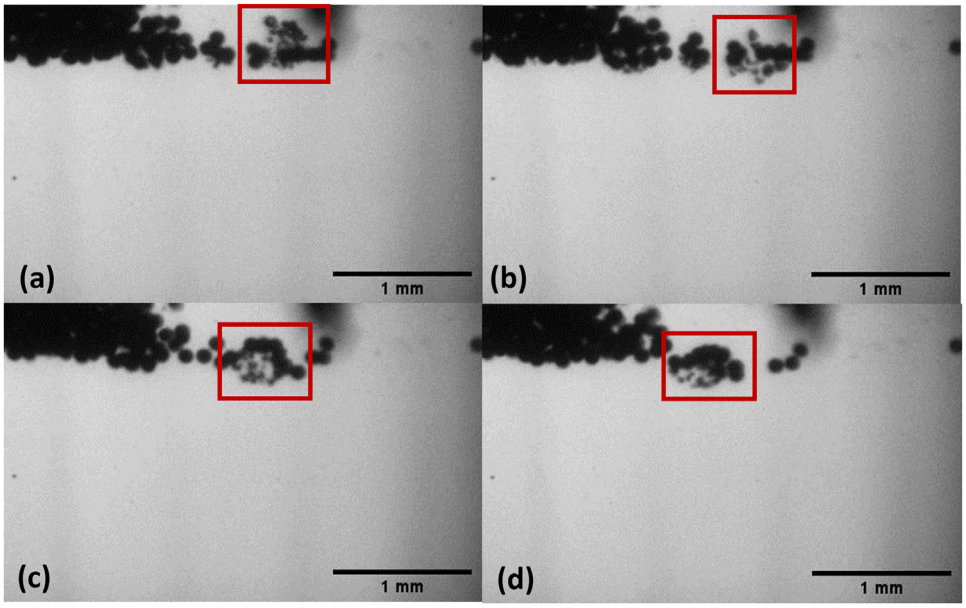

Figure 4. (a–d) Formation and movement of a Sonovue microbubble cloud (Video S3), driven at 0.5 MHz, 2.8 MPa peak negative focal pressure, 5% duty cycle and 3.3 Hz pulse repetition frequency. Microspheres (106 μm diameter) can be seen moving towards the cloud (*red outlined section*) and travelling with it before rebounding off the cavity edge. Images were captured at 4 × magnification, at 100,000 fps. The direction of ultrasound propagation is from the top to the bottom of each image.

of cavitation structures in single fluids such as acoustic Lichtenburg figures [27].

Prior to the extravasation of microspheres and the formation of channels, an oscillation or "rippling" of the agar:water interface was seen at the edge of the well (Fig. 3). Increasing the magnification (10 ×) and imaging frame rate (100,000 frames/s) indicated that this movement was owing to the formation and motion of a microbubble cloud (Fig. 3; Video S2, online only). In Figure 4 and the corresponding video (Video S3, online only), the microbubble cloud can be seen travelling and to consist of a combination of microbubbles and associated microspheres (indicated by the *red rectangle*). Microspheres can be seen being drawn towards the cloud and rebounding off its surface.

In each experiment, multiple clouds were observed travelling to the front of the cavity over the course of ultrasound exposure (Video S4, online only). This resulted in the formation of a large broad singular channel, approximately equal in width to that of the transducer focal

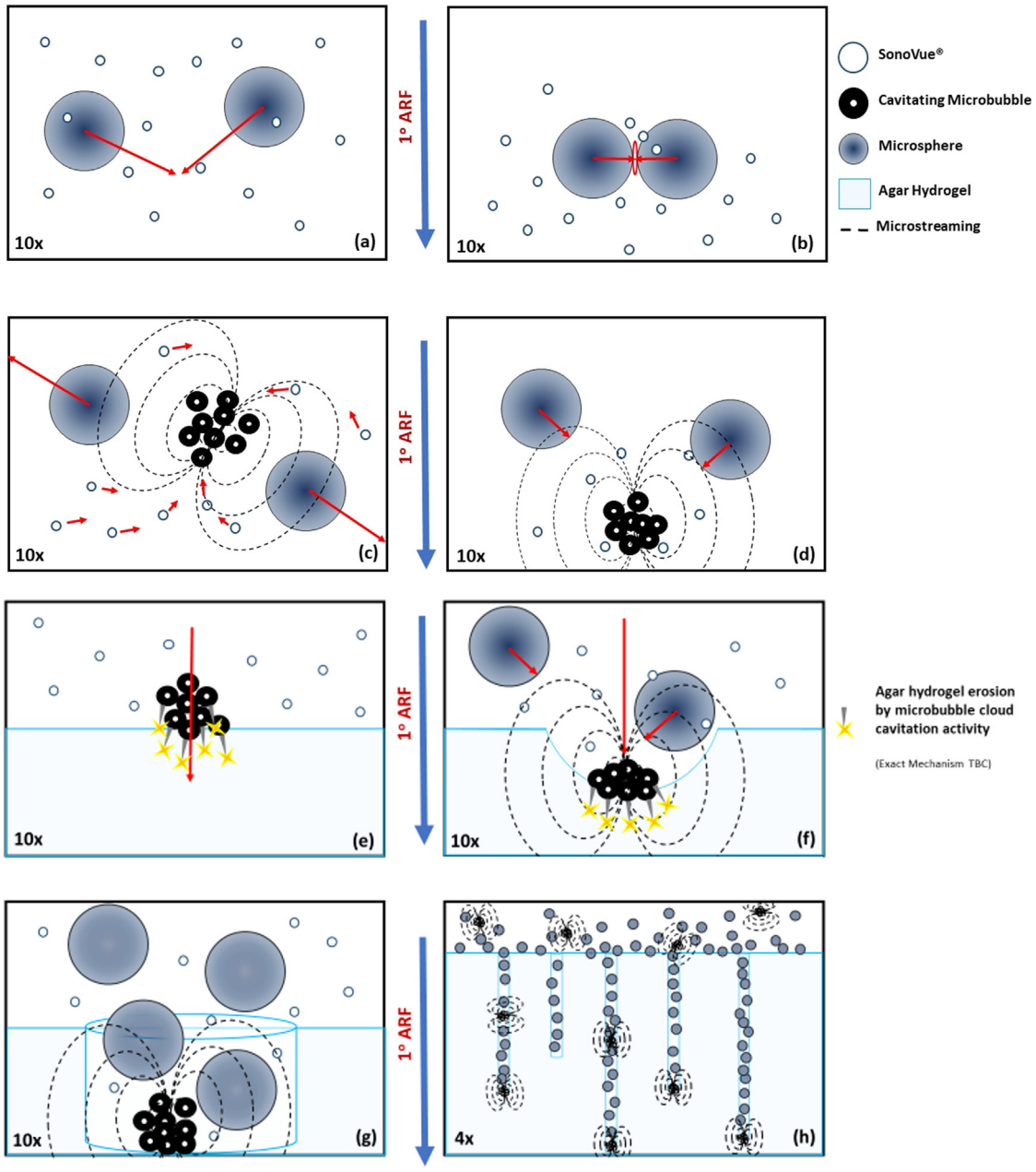

Figure 5. Graphical summary of mechanisms leading to microsphere extravasation in a hydrogel tissue phantom. Secondary acoustic radiation forces (ARFs) between oscillating SonoVue microbubbles lead to the formation of microbubble clouds (a). Microsphere collisions (b) brought about by the action of primary ARF and/or microstreaming promote formation of additional bubble clouds (c), which then dissociate from the microspheres and move towards the hydrogel boundary interface under the primary ARF. Individual microbubble oscillations within the microbubble cloud produce secondary ARFs, which draw in nearby microspheres, promoting additional collisions (d). Microbubble clouds are propelled towards the agar boundary surface by the primary ARF (e). The oscillating microbubble clouds cause mechanical erosion of the agar (f), producing channels within it that are filled with microspheres via a combination of microstreaming and ARF (g). Further microsphere collisions occur, producing additional bubble clouds and extending the channels. These events occur at multiple locations throughout the cavity, producing multiple microbubble clouds and corresponding channels (h). Ultrasound propagation is from top to bottom in all image panels. Objects are not to scale but the approximate magnification corresponding to the high-speed videos is indicated in the lower left-hand corner of all image panes. *Red arrows* denote the direction of microsphere and/or microbubble movement. *Dotted lines* indicate microstreaming.

region (1 mm for 0.5 MHz). It is difficult to ascertain with absolute certainty how many clouds are formed, expire, coalesce or are sustained throughout the time captured, as at these frame rates (100,000 −200,000 fps) and magnification, it is not possible to temporally or spatially resolve oscillations of individual microbubbles within the cloud; nor is it possible to record the activity of the microbubble cloud over the entire pulse length at this capture rate because of the maximum number of frames allowed using the HPV-X2 (256 frames).

Figure 5 summarises the observed phenomena and hypothesised mechanisms underpinning microsphere extravasation. Multiple phenomena appear to be involved: Cloud formation seemingly occurred either as the result of secondary radiation forces causing attraction of pre-existing SonoVue microbubbles and/or collision of microspheres promoting nucleation of multiple bubbles (potentially from sub-micrometre bubbles present in the SonoVue suspension). Secondary radiation forces are also likely to have been responsible for the movement of the microspheres towards the microbubble clouds. Erosion of the agar may have been the result of direct impingement of the microbubble clouds moving under the action of the primary radiation force [28,29]. In the experiments performed with smaller microspheres at the lower peak negative pressure (1.9 MPa), the channels produced were similar to the "tunnels" reported in previous microbubble studies [30] and attributed to primary radiation force.

Some of the observed microsphere movement also indicated that microstreaming was occurring (Video S5, online only), which could have imposed shear stresses upon the nearby surface and facilitated the removal of material from it [31]. Microjetting, which has been widely associated with erosion of surfaces in cavitation studies [32–34], may also have played a role although this was not directly observed. Gerold et al. [35] have reported extensive jetting from microbubble clouds; and whilst microjets are expected to travel towards the most rigid adjacent surface (which in this case would be the glass microspheres rather than the agar), the convex surface of the microspheres may have promoted counterjet formation [36].

Interestingly formation of microbubble clouds was generated in some cases apparently as the result of collision of the glass microspheres (Video S5). This is potentially because contact between the two curved surfaces creates a nucleation site between the two microspheres [11,37]. Once formed, the new clouds appear to grow and drive the microspheres apart, enabling the cloud to travel in the direction of ultrasound propagation and further promoting the movement of the microspheres.

Limitations

This was a preliminary study to establish the feasibility of using cavitation to promote microsphere transport. The agar–agar phantom was designed to mimic a relatively soft malignant tissue and does not accurately represent the wide range of tissue properties that exist *in vivo*. Further work is required to confirm that equivalent microsphere transport could be achieved in real tissue and the degree to which tissue inhomogeneity would influence the distribution of microspheres that could be achieved.

The correlation between channel length and ultrasound exposure duration and the alignment of the majority of the channels with the direction of ultrasound propagation indicates that spatial control of microsphere distribution would be feasible. Achieving a uniform distribution in three dimensions around a post-resection cavity or blood vessel would require significant manipulation of the beam, which could be challenging for some applications, and again would be affected by tissue homogeneity.

The SonoVue concentration used was much higher than could be achieved in the circulation (although it would be feasible in a post-resection cavity), and further work would be needed to determine the effect of microbubble concentration on microsphere transport.

Conclusions

The results of this study illustrate that ultrasound-induced cavitation can promote the transport of microspheres in the range 15–107 μm in a tissue-mimicking phantom. High-speed optical imaging indicated that the formation of channels in the phantom was the result of erosion produced by clouds of oscillating microbubbles propelled by the primary acoustic radiation force. Microsphere transport was promoted by a combination of primary and secondary acoustic radiation forces and microstreaming, enabling the microspheres to travel into the channels with the bubble clouds. This is in contrast to the mechanisms proposed to explain the transport of small molecule drugs and nanoparticles, which are thought to relate primarily to the action of single microbubbles creating pores in biological membranes and enhancing convection. It was also observed that collisions of microspheres appeared to promote bubble nucleation, increasing the number of microbubble clouds produced. The total length of the channels was found to be influenced primarily by the total ultrasound exposure time. Further work is needed to determine whether comparable transport can be achieved in biological tissue and the effect of changing other experimental parameters.

Declaration of competing interest

When the study was initially conceived, J.V. and A.L. were employees of Boston Scientific through whom a patent was filed on ultrasound-enhanced microsphere transport and on which all authors are listed as inventors. Boston Scientific, however, had no influence on the design of the study, its conduct or preparation of this article.

Acknowledgments

The authors are grateful to the Royal Commission for the Exhibition of 1851 for funding J.V. on an industrial fellowship and to Boston Scientific for the provision of glass microspheres. The authors also thank James Fisk and David Salisbury for construction of the apparatus used in this study, and Dr. Bernard Shieh for his assistance with the simulations included in the supplementary material.

Data availability statement

All of the data obtained in this study have been made available in the supplementary material and at the Oxford University Research Archive at https://ora.ox.ac.uk/objects/uuid:b0f3731d-fc5b-4ef2-bc78-cde2fd808aa9.

Supplementary materials

Supplementary material associated with this article can be found in the online version at doi:10.1016/j.ultrasmedbio.2023.01.025.

References

[1] Kooiman K, Roovers S, Langeveld SAG, Kleven RT, Dewitte H, O'Reilly MA, et al. Ultrasound-responsive cavitation nuclei for therapy and drug delivery. Ultrasound Med Biol 2020;46:1296–325.
[2] Labbaf S, Horsley H, Chang MW, Stride E, Malone-Lee J, Edirisinghe M, et al. An encapsulated drug delivery system for recalcitrant urinary tract infection. J R Soc Interface 2013;10:20130747.
[3] Mannaris C, Bau L, Grundy M, Gray M, Lea-Banks H, Seth A, et al. Microbubbles, nanodroplets and gas-stabilizing solid particles for ultrasound-mediated extravasation of unencapsulated drugs: an exposure parameter optimization study. Ultrasound Med Biol 2019;45:954–67.
[4] Lee JY, Carugo D, Crake C, Owen J, De Saint, Victor M, Seth A, et al. Nanoparticle-loaded protein–polymer nanodroplets for improved stability and conversion efficiency in ultrasound imaging and drug delivery. Adv Mater 2015;27:5484–92.
[5] Lee JY, Crake C, Teo B, Carugo D, de Saint, Victor M, Seth A, et al. Ultrasound-enhanced siRNA delivery using magnetic nanoparticle-loaded chitosan-deoxycholic acid nanodroplets. Adv Healthc Mater 2017;6.

[6] Bazan-Peregrino M, Rifai B, Carlisle RC, Choi J, Arvanitis CD, Seymour LW, et al. Cavitation-enhanced delivery of a replicating oncolytic adenovirus to tumors using focused ultrasound. J Control Release 2013;169:40–7.
[7] Kwan JJ, Lajoinie G, De Jong N, Stride E, Versluis M, Coussios CC. Ultrahigh-speed dynamics of micrometer-scale inertial cavitation from nanoparticles. Phys Rev Appl 2016;6:1–8.
[8] Yemane PT, Åslund AKO, Snipstad S, Bjørkøy A, Grendstad K, Berg S, et al. Effect of ultrasound on the vasculature and extravasation of nanoscale particles imaged in real time. Ultrasound Med Biol 2019;45:3028–41.
[9] Azmin M, Mohamedi G, Edirisinghe M, Stride EP. Dissolution of coated microbubbles icrobubbles crobubbles : The effect of nanoparticles and conMater. Sci Eng C 2012;32:2654–8.
[10] Il Yoon Y, X Pang, Jung S, Zhang G, Kong M. Smart gold nanoparticle-stabilized ultrasound microbubbles as cancer theranostics. J Mater Chem B 2018;6:3235–9.
[11] Borkent BM, Gekle S, Prosperetti A, Lohse D. Nucleation threshold and deactivation mechanisms of nanoscopic cavitation nuclei. Phys Fluids 2009;21:102003.
[12] Roos ST, Juffermans LJM, van Royen N, van Rossum AC, Xie F, Appelman Y, et al. Unexpected high incidence of coronary vasoconstriction in the Reduction of Microvascular Injury Using Sonolysis (ROMIUS) Trial. Ultrasound Med Biol 2016;42:1919–28.
[13] Sheng Y, Beguin E, Nesbitt H, Kamila S, Owen J, Barnsley LC, et al. Magnetically responsive microbubbles as delivery vehicles for targeted sonodynamic and antimetabolite therapy of pancreatic cancer. J Control Release 2017;262:192–200.
[14] Eisenbrey JR, Shraim R, Bin Liu J, Li J, Stanczak M, Oeffinger B, et al. Sensitization of hypoxic tumors to radiation therapy using ultrasound-sensitive oxygen microbubbles. Int J Radiat Oncol Biol Phys 2018;101:88–96.
[15] Wu CH, Liu HL, Ho CT, Hsu PH, Fan CH, Yeh CK, et al. Monitoring of acoustic cavitation in microbubble-presented focused ultrasound exposure using gradient-echo MRI. J Magn Reson Imaging 2020;51:311–8.
[16] Aryal M, Arvanitis CD, Alexander PM, McDannold N. Ultrasound-mediated blood–brain barrier disruption for targeted drug delivery in the central nervous system. Adv Drug Deliv Rev 2014;72:94–109.
[17] Mainprize T, Lipsman N, Huang Y, Meng Y, Bethune A, Ironside S, et al. Blood–brain barrier opening in primary brain tumors with non-invasive MR-guided focused ultrasound: a clinical safety and feasibility study. Sci Rep 2019;9:321.
[18] Lipsman N, Meng Y, Bethune AJ, Huang Y, Lam B, Masellis M, et al. Blood–brain barrier opening in Alzheimer's disease using MR-guided focused ultrasound. Nat Commun 2018;9:2336.
[19] Abrahao A, Meng Y, Llinas M, Huang Y, Hamani C, Mainprize T, et al. First-in-human trial of blood–brain barrier opening in amyotrophic lateral sclerosis using MR-guided focused ultrasound. Nat Commun 2019;10:4373.
[20] Huang P, Zhang Y, Chen J, Shentu W, Sun Y, Yang Z, et al. Enhanced antitumor efficacy of ultrasonic cavitation with up-sized microbubbles in pancreatic cancer. Oncotarget 2015;6:20241–51.
[21] Kotopoulis S, Dimcevski G, Gilja OH, Hoem D, Postema M. Treatment of human pancreatic cancer using combined ultrasound, microbubbles, and gemcitabine: a clinical case study. Med Phys 2013;40:72902.
[22] Dimcevski G, Kotopoulis S, Bjanes T, Hoem D, Schjøt J, Gjertsen BT, et al. A human clinical trial using ultrasound and microbubbles to enhance gemcitabine treatment of inoperable pancreatic cancer. J Control Release 2016;243:172–81.
[23] Eisenbrey JR, Forsberg F, Wessner CE, Delaney LJ, Bradigan K, Gummadi S, et al. US-triggered microbubble destruction for augmenting hepatocellular carcinoma response to transarterial radioembolization: a randomized pilot clinical trial. Radiology 2021;298:450–7.
[24] Stewart DC, Rubiano A, Dyson K, Simmons CS. Mechanical characterization of human brain tumors from patients and comparison to potential surgical phantoms. PLoS One 2017;12:1–19.
[25] Lea-Banks H, Teo B, Stride E, Coussios CC. The effect of particle density on ultrasound-mediated transport of nanoparticles. Phys Med Biol 2016;61:7906–18.
[26] Marmottant P, Hilgenfeldt S. Controlled vesicle deformation and lysis by single oscillating bubbles. Nature 2003;423:153–6.
[27] Li F, Zhang X, Tian H, Hu J, Chen S, Mo R, et al. Interactions of bubbles in acoustic Lichtenberg figure. Ultrason Sonochem 2022;87:106057.
[28] Hendley SA, Bollen V, Anthony GJ, Paul JD, Bader KB. *In vitro* assessment of stiffness-dependent histotripsy bubble cloud activity in gel phantoms and blood clots. Phys Med Biol 2019;64:145019.
[29] Acconcia C, Leung BY, Manjunath A, Goertz DE. Interactions between individual ultrasound-stimulated microbubbles and fibrin clots. Ultrasound Med Biol 2014;40:2134–50.
[30] Caskey CF, Qin S, Dayton PA, Ferrara KW. Microbubble tunneling in gel phantoms. J Acoust Soc Am 2009;125:EL183.
[31] Leighton TG. Acoustic bubble. London: Academic Press; 1994. p. 439–590.
[32] Brujan EA. The role of cavitation microjets in the therapeutic applications of ultrasound. Ultrasound Med Biol 2004;30:381–7.
[33] Shao JL, Wang P, He AM. Influence of shock pressure and profile on the microjetting from a grooved Pb surface. Model Simul Mat Sci Eng 2017;25:1–19.
[34] Lechner C, Koch M, Lauterborn W, Mettin R. Pressure and tension waves from bubble collapse near a solid boundary: a numerical approach. J Acoust Soc Am 2017;142:3649–59.
[35] Gerold B, Rachmilevitch I, Prentice P. Bifurcation of ensemble oscillations and acoustic emissions from early stage cavitation clouds in focused ultrasound. New J Phys 2013;15:033044.
[36] Tomita Y, Robinson PB, Tong RP, Blake JR. Growth and collapse of cavitation bubbles near a curved rigid boundary. J Fluid Mech 2002;466:259–83.
[37] Atchley AA, Prosperetti A. The crevice model of bubble nucleation. J Acoust Soc Am 1989;86:1065–84.